LASER APPLICATIONS AND OTHER TOPICS IN QUANTUM ELECTRONICS PACS numbers: 42.79.Qx; 42.55.Lt
DOI: 10.1070/QE2005v035n06ABEH003465

Calculation of optimal parameters of an NH_2-CO_2 lidar

B.I. Vasil'ev, O.M. Mannoun

***Abstract*. The basic parameters (range, signal-to-noise ratio, and sensitivity) of a lidar using NH_3 and CO_2 lasers are calculated. The principle of lidar operation is based on the differential absorption recording. Absorption spectra of all known Freons are considered in the spectral range 9 – 13.5 μm and optimal wavelengths suitable for sensing them are determined. It is shown that the NH_3-CO_2 lidar can sense Freons at distances up to 10 km at a signal-to-noise ratio exceeding 10. Sensitivities of the lidar for sensing Freon-11 using various lines of the ammonia laser are calculated. It is shown that remote sensing of Freon-11 at concentrations of the order of 5×10^{-6} % is possible at distances up to 8.5 km.**

Keywords: *NH_3-CO_2 lidar, differential absorption, Freons.*

1. Introduction

The development of a high-power ammonia laser [1] emitting in the range 11 – 13.5 μm opened new possibilities for atmospheric sensing in the transparency window 8 – 14 μm. The use of the ammonia laser in lidar systems was first proposed in paper [2]. Later, a lidar based on NH_3 laser with a nonselective cavity and capable of operating simultaneously at several spectral lines in the range 11 – 13 μm (which is undoubtedly an advantage of such a system) was considered in [3]. However, the number of lines emitted by the laser operation in such a regime is limited and the energy of each line is lower than for a laser with a selective cavity, which reduces the number of gases that can be detected as well as the range of their sensing. The optical scheme of a two-frequency ammonia lidar was proposed in [4], but the laser beam control system was found to be impractical, especially for mobile lidars. To overcome this problem, an optical scheme of a two-frequency ammonia lidar was proposed in [5], in which the output beams of the ammonia laser are collinear and can be controlled more easily. A new optical scheme of a two-frequency emitter based on carbon dioxide and ammonia lasers was proposed in [6] to cover the spectral range 9 – 13.5 μm.

A differential absorption lidar (DIAL) based on a CO_2 laser, which was used by various research groups [7 – 9], is most popular for atmospheric sensing in the transparency window 8 – 14 μm. The CO_2 laser tuning range ($\lambda = 9 - 11$ μm) covers the absorption lines of over 90 gases including NH_3, C_2H_2, H_2O, O_3, CO_2, N_2O, NO_2, HNO_3, SF_6, OSC, CS_2, hydrozine, rocket fuel and chemical agents [10]. Additional application of an ammonia laser ($\lambda = 11 - 13.5$ μm) further increases the range of DIAL sensing in the atmospheric transparency window 8 – 14 μm. This wavelength range covers strong absorption bands of many gases that are not accessible for detection by the CO_2 laser, e.g., Freons, organic gases and chemical agents [11].

In this paper, we consider the main parameters (range, signal-to-noise ratio, and sensitivity) of DIALs in which NH_3 and CO_2 lasers are employed [6]. The lidar parameters were studied only in the NH_3 laser range. For comparison, we used lidar parameters in the CO_2 laser range which were optimised in [12 – 15].

2. Description of a lidar

The differential absorption method (DAM) is used for atmospheric sensing by an NH_3-CO_2 lidar. This method is based on resonant absorption in the investigated gas whose concentration is calculated by recording two signals at two wavelengths, one of which (λ_{on}) lies in the range of the absorption line of the investigated gas and the other (λ_{off}) lies outside this line. Two schemes are used for the lidar operation, one employing a topographic reflector or a retroreflecting mirror, and the other using the atmospheric aerosol as the reflector. We shall consider only the second scheme which allows us to measure the concentration of the investigated gas with spatial resolution.

The emission spectra of NH_3 and CO_2 lasers presented in Fig. 1 show that the pulse energy of the CO_2 laser is slightly higher than the pulse energy of the ammonia laser. This difference is due to the high efficiency of the ammonia laser whose maximum value is 21 % for the aP(4, 0) line ($\lambda = 11.71209$ μm) [1]. The ammonia laser is pumped by a CO_2 laser [the 9R(30) line, $\lambda = 9.22$ μm] and generates at more than 30 lines in the range 11 – 13.5 μm. In order to realise the DAM, the 9R(30) line of the CO_2 laser is used as the reference line (λ_{off}), while any of the NH_3-laser lines serves as the sensing line (λ_{on}).

B.I. Vasil'ev P.N. Lebedev Physics Institute, Russian Academy of Sciences, Leninskii prosp. 53, 119991 Moscow, Russia;
e-mail: bvasil@sci.lebedev.ru
O.M. Mannoun Moscow Institute of Physics and Technology (State University), Institutskii per. 9, 141700 Dolgoprudnyi, Moscow region, Russia

Received 11 January 2005
Kvantovaya Elektronika **35** (6) 563 – 568 (2005)
Translated by M.N. Sapozhnikov

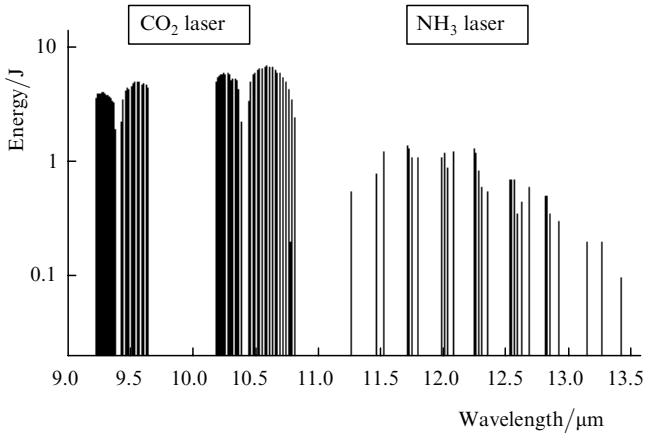

Figure 1. Lasing spectrum of NH_3-CO_2 emitter.

Note that the CO_2 laser generates more than 60 lines which can also be used for sensing. The optical scheme proposed in [6] allows simultaneous use of NH_3 and CO_2 lasers working in the 11–13.5 μm and 9 – 11 μm ranges, respectively. A Michelson interferometer with diffraction gratings as reflectors is used as the output mirror in the CO_2 laser, and hence the realisation of the DAM requires a tuning of the output diffraction gratings of the Michelson interferometer simultaneously at two lines with λ_{on} and λ_{off}.

Table 1 contains a list of all Freons having absorption bands in the emission region of the ammonia laser, optimal lines for sensing these Freons and the Freon absorption cross section at these lines. The data shown in Table 1 are borrowed from the HITRAN-2000 atlas [11]. The absorption cross sections were calculated in atmosphere at a temperature of 296 K and at a pressure of 1 atm. Note that the absorption spectra of Freon-11 and Freon-12 lie in the emission range of the CO_2 laser also, hence these gases were sensed by lidars based on the CO_2 laser [16]. However, the absorption cross sections of these gases in the indicated frequency range are one-fourth of those in the ammonia laser range [11]. It follows hence that the application of a lidar in the spectral range 11 – 13.5 μm is more efficient.

An important property of the ammonia laser for atmospheric sensing is its narrow line. The gain linewidth $\Delta\nu$ of the ammonia laser is determined by the expression [17]

$$\Delta\nu = 28p_{NH_3} + 3.8p_{N_2},$$

where $\Delta\nu$ is measured in megahertz and the pressure p_i in Torrs. For the optimal composition $NH_3 : N_2 = 1 : 75$ of the active medium of the ammonia laser at a total pressure of 60 Torr, we have $\Delta\nu = 247$ MHz. For the TEA CO_2 laser, the gain linewidth lies in the range 3 – 4 GHz, depending on the mixture composition and its pressure.

The main interfering gases that may be present in the atmosphere during sensing in the wavelength range 9 – 13.5 μm are O_3, C_2H_4, NH_3, CO_2 and H_2O. Ethylene (C_2H_4) does not have an absorption band in the ammonia laser range, and its absorption cross section in the CO_2 laser range varies in the interval $0.1 - 32\ cm^{-1}\ atm^{-1}$ [11, 18]. The largest absorption cross sections of ozone and ammonia [19] in the CO_2 laser range are about double the value in the ammonia laser range [11]. For water vapour, the difference in these cross sections is always insignificant except for the region in the vicinity of $\lambda = 11.7$ μm, where the atmospheric attenuation coefficient at the aP(4, 2) line is $0.446\ km^{-1}$. The transmission of the atmosphere at the edge of the transparency window used for $\lambda > 13$ μm is low and is determined by the absorption by carbon dioxide gas. Hence, the atmospheric attenuation coefficient at the aP(9, 7) and aP(7, 3) lines is 0.9552 and $0.9953\ km^{-1}$, respectively [20]. At the remaining lines of the ammonia laser, the atmospheric transmission is comparable with the transmission of the CO_2 laser radiation.

3. Basic lidar equations

3.1 Lidar signal

In the single elastic scattering approximation, the lidar equation has the form [21]

$$P_\lambda(z) = P_0\frac{c\tau_p}{2}\eta_a(\lambda)\frac{A_t(z)}{z^2}\beta_\lambda(z)\exp\left[-2\int_0^z \alpha_\lambda(\xi)d\xi\right], \quad (1)$$

where z is the distance from the scattering volume (range); c is the velocity of light; τ_p is the laser pulse duration; P_λ is the scattering radiation power; P_0 is the laser power; η_a is the efficiency of the detector; β_λ is the volume coefficient of

Table 1.

Gas	Chemical formula	Spectral range/μm	NH_3-laser line	Absorption cross section/$cm^{-1}atm^{-1}$
Freon-11	CCl_3F	11.364 – 12.346	sP(6, K)	115.7
Freon-12	CCl_2F_2	10.526 – 11.765	aP(3, 1)	6.55
Freon-13	$CClF_3$	12.423 – 13.072	aP(7, 4)	5.77
Freon-21	$CHCl_2F$	11.905 – 12.739	aP(6, 3)	25.11
Freon-22	$CHClF_2$	11.628 – 13.158	aP(6, 0)	17.64
Freon-113	$C_2Cl_3F_3$	10.050 – 12.812	aP(6, 2)	36.35
Freon-114	$C_2Cl_2F_4$	11.628 – 12.270	aP(4, 0)	22.52
Freon-123	CF_3CHCl_2	11.111 – 13.515	aP(5, 2)	16.09
Freon-124	$CHClF_2CF_3$	10.869 – 12.657	aP(6, 4)	5.53
Freon-125	CHF_2CF_3	11.236 – 11.905	sP(5, K)	11.3
Freon-141	CH_3CCl_2F	12.658 – 14.085	aP(9, 6)	27.26
Freon-142	CH_3CClF_2	7.905 – 11.429	sP(4, K)	6.4
Freon-143	CF_3CH_3	9.525 – 13.334	aP(5, 4)	3.58
Freon-152	CH_3CHF_2	10.050 – 11.905	aP(7, 1)	2.74
Freon-225	$CClF_2CF_2CHClF$	11.561 – 14.389	aP(5, 1)	11.13

the atmospheric backscattering; A_t is the effective area of the detector; and α_λ is the coefficient of bulk attenuation (extinction) by the atmosphere. The efficiency η_a of the detector is determined by the transmission of the transmitting (q_t) and receiving (q_r) optical systems and the efficiency χ of the photodetector: $\eta_a = q_t q_r \chi(1 - q_l)$, where q_l are other losses in the receiver–detector channel.

The extinction coefficient α_λ may be presented as the sum of terms describing the molecular (α_λ^{mol}) and aerosol (α_λ^{aer}) attenuation: $\alpha_\lambda = \alpha_\lambda^{aer} + \alpha_\lambda^{mol}$. The molecular extinction coefficient α_λ^{mol} includes attenuation due to absorption by the gas being studied ($\alpha_\lambda^g = N_g \sigma_\lambda^g$, where N_g is the gas concentration and σ_λ^g is its absorption cross section at the wavelength λ). The backscattering coefficient β_λ can also be presented as the sum of two terms describing molecular (β_λ^{mol}) and aerosol (β_λ^{aer}) scattering: $\beta_\lambda = \beta_\lambda^{aer} + \beta_\lambda^{mol}$. The molecular scattering coefficient β_λ^{mol} and molecular extinction coefficient α_λ^{mol} can be calculated to a high degree of accuracy using the Rayleigh scattering theory [22] or the atmosphere model proposed in [20, 23]. The aerosol scattering coefficient β_λ^{aer} and the aerosol extinction coefficient α_λ^{aer}can be determined either theoretically using the Mie aerosol scattering theory [22] or experimentally from lidar signals using the algorithm for solving the lidar equation [24].

The effective area $A_t(z)$ of the detector is described by the equation [21]

$$A_t(z) = \frac{A_0}{\pi W^2(z)} \times \int_{r=0}^{r_t} \int_{\psi=0}^{2\pi} \xi(z,r,\psi) F(z,r,\psi) r \, dr d\psi = A_0 \xi(z), \quad (2)$$

where $F(z,r,\psi)$ is the laser radiation distribution function; $\xi(z,r,\psi)$ is the geometrical probability factor; $W(z)$ is the size of the laser spot at a distance z (in the plane of the object); A_0 is the input aperture area of the telescope; $\xi(z)$ is the function of the geometrical lidar factor accounting for the fraction of the laser beam reflected at the target; r_t is the diameter of the input aperture of the telescope; and r, ψ are polar coordinates.

3.2 Signal-to-noise ratio

In our lidar working on direct detection principle, in which the Schottky noise of the detector is the main limiting factor, the signal-to-noise ratio is calculated from the formula [21]

$$\mathrm{SNR} = \frac{P_\lambda}{[2B(P_f + P_\lambda)hv/\eta + BP_d^2]^{1/2}}, \quad (3)$$

where η is the quantum efficiency of the detector; hv is the photon energy; P_d is the power equivalent to the detector noise power; B is the electron transmission band width of the detector; and P_f is the background radiation power of the atmosphere.

The power equivalent to the detector noise power and the background radiation power of the atmosphere can be described by the expressions [21]

$$P_d = \frac{\sqrt{S_d}}{D^*}, \quad (4)$$

$$P_f = B_\lambda A_0 q_r \pi \theta_t^2 \Delta\lambda, \quad (5)$$

where S_d is the sensitive area of the detector and D^* is its detectivity; $2\theta_t$ is the field-of-view angle of the telescope; $\Delta\lambda$ is the transmission width of the optical filter; and B_λ is the spectral radiance of the atmospheric background, varying from 1 to 300 W m^{-2} sr^{-1} μm^{-1} [25].

3.3 Sensitivity of the lidar

The sensitivity S of a lidar is the minimum concentration of the gas that can be measured by it with a certain spatial resolution at a certain range for a relative error equal to 100 %. The classical formula for the relative error δN in determining the average gas concentration by the differential absorption method in a certain spatial interval can be presented in the form [26]

$$\delta N = \frac{1}{2\Delta\sigma\Delta R}\left[\frac{2}{N_p}(\delta_{on}^2 + \delta_{off}^2) + \delta_S^2\right]^{1/2}, \quad (6)$$

where ΔR is the spatial resolution of the lidar, whose minimum value is determined by the duration of the laser sensing pulse ($\Delta R = c\tau_p/2$); N_p is the number of pulses in a series; δ_{on} and δ_{off} are the random errors in detecting signals at wavelengths λ_{on} and λ_{off}; δ_S is the systematic error not connected with the detector noise; $\Delta\sigma = \sigma(\lambda_{on}) - \sigma(\lambda_{off}) = \sigma_{on} - \sigma_{off}$ is the differential absorption cross section of the gas being investigated; and σ_{on} and σ_{off} are the absorption coefficients inside and outside the absorption line, respectively. The values of δ_{on} and δ_{off} are usually computed through the signal-to-noise ratio. The expression for the systematic error has the form [27]

$$\delta_S^2 = 2(\delta_{\beta aer}^2 + \delta_{\beta mol}^2)\left(\frac{\beta_{off}^{aer}\beta_{on}^{mol} - \beta_{on}^{aer}\beta_{off}^{mol}}{\beta_{off}\beta_{on}}\right) + (2\Delta R)^2[(\alpha_{on}^{aer} - \alpha_{off}^{aer})^2\delta_{\alpha aer}^2 + (\alpha_{on}^{mol} - \alpha_{off}^{mol})^2\delta_{\alpha mol}^2] + (2\Delta R)^2\sum_{j=1}^{M}\left(\Delta\sigma_j^2\delta_{N_j}^2 + \delta_{\Delta\sigma_j}^2 N_j^2\right) + (2\Delta\sigma\Delta R)^2\delta_{\Delta\sigma}^2, \quad (7)$$

where $\delta_{\beta aer}$ and $\delta_{\beta mol}$ are the relative errors in determining the coefficients of backward scattering by aerosol particles and molecules of the atmosphere, respectively; $\delta_{\alpha aer}$ and $\delta_{\alpha mol}$ are the relative errors associated with the absorption of laser radiation by aerosol particles and molecules of the atmosphere, respectively; δ_{N_j} and $\delta_{\Delta\sigma_j}$ are the relative errors in specifying or determining the concentration N_j of the jth interfering gas and its differential absorption coefficient $\Delta\sigma_j$; and $\delta_{\Delta\sigma}$ is the relative error in specifying or determining the differential absorption coefficient of the gas being investigated.

The first two terms in relation (7) are connected with the variation of scattering properties of the medium during tuning of the wavelength. The third term must be considered if interfering gases are present. The last term is connected with the error in determining or specifying the absorption cross section of the gas under study.

4. Results of calculations

The following are the main technical parameters used in our calculations:

Emitter

Spectral range	9–11 μm 11–13.5 μm
Pulse energy E_p	to 5 J to 1.5 J
Pulse duration τ_p	1 μs
Divergence after beam expander (telescope)	0.8 mrad
Beam diameter at the exit from the expander	10 cm
Beam expander efficiency q_t	70 %

Telescope

Type	Newtonian telescope
Telescope aperture diameter	40 cm
Focal length	1 m
Field of view $2\theta_t$	1 mrad
Distance between the laser axis and the telescope axis	50 cm
Efficiency q_r of the telescope	80 %

Detector

Type	KRT cooled to 77 K
Sensing area	0.5×0.5 mm
Detecting power D^*	2×10^{11} cm $Hz^{1/2}$ W^{-1}
Optical filter transmission width $\Delta\lambda$	4 nm
Electronic transmission band width B	1 MHz
Efficiency χ	50 %
Time constant	$\leqslant$ 10 ns

We also used vertical concentration profiles of gas components in the natural atmosphere, which are presented in the form of various statistical models of cloudless atmosphere, namely, tropical, midlatitude summer, midlatitude winter, subarctic summer, subarctic winter, and standard. Data on these profiles, as well as on the temperature and pressure stratification models were borrowed from the AFGL/MODTRAN 3 atlas [20]. To calculate the geometrical factor function of the lidar, we used algorithms proposed in [28]. Spectral data for gases were borrowed from the HITRAN-2000 atlas [11].

4.1 Lidar range

In order to determine the range of a lidar, we calculated the signal-to-noise ratio for various ammonia laser lines whose characteristics are presented in Table 2. The results of calculations, which are presented in Fig. 2, show that the lidar may carry out atmospheric sensing for a signal-to-noise ratio exceeding 10 at distances from 3.5 km [aP(7, 3) line] to 8.5 km [aP(5, K) line]. Calculations were made using the standard atmospheric model along a horizontal track at sea level, where the average coefficient of aerosol back scattering $\beta^{aer} = 2.17 \times 10^{-6}$ m^{-1} sr^{-1} [20].

The effect of atmospheric conditions was studied by calculating the signal-to-noise ratio for the most intense ammonia laser line aP(4, 0) (pulse energy $E_p = 1.4$ J, laser efficiency 21 %) using various models of the atmosphere [20]. The results of computations, which are presented in Fig. 3, show that the lidar range is the lowest in the tropical atmosphere and amounts to 4.5 km for a signal-to-noise ratio exceeding 10, while the highest range of lidar is observed in the subarctic winter atmosphere and may cover 10 km for the same signal-to-noise ratio (under conditions when such a value is sufficient for measurements).

Table 2.

Line	λ/μm	E_p/J	α_λ/km^{-1}
sP(2, 1)	10.7732	0.1	0.041
sP(5, K)	11.5207	1.25	0.062
aP(4 0)	11.7121	1.4	0.091
aP(4, 2)	11.7271	1.3	0.44
aP(7, 3)	12.5607	0.7	0.55

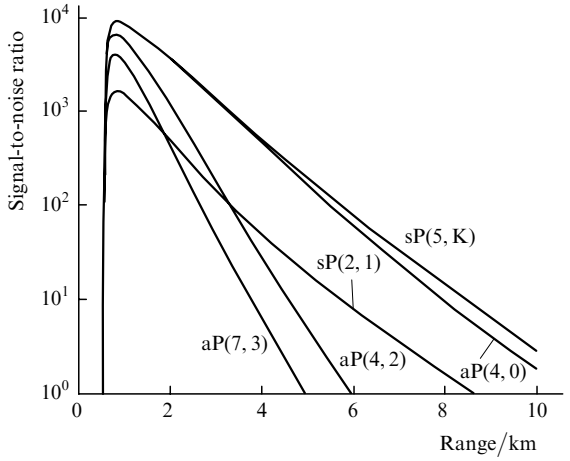

Figure 2. Signal-to-noise ratio for different lines of ammonia laser.

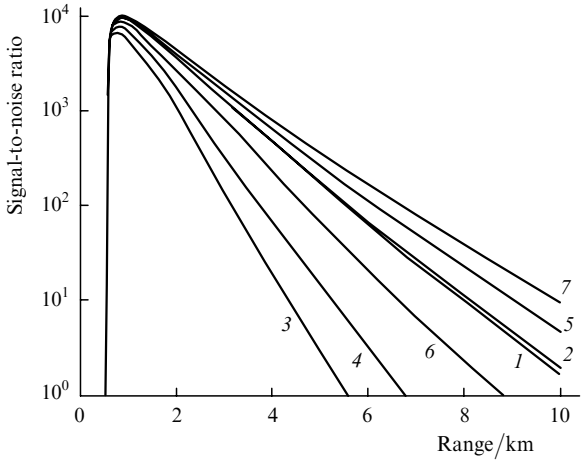

Figure 3. Signal-to-noise ratio for the aP(4, 0) line for various atmospheric models: standard (*1*), at a temperature of 296 K and a pressure of 1 atm (*2*); tropical (*3*); midlatitude summer (*4*); midlatitude winter (*5*); subarctic summer (*6*); subarctic winter (*7*).

The results presented above lead to the conclusion that the maximum sensing range R_{max} of ammonia laser is attained in subarctic winter atmosphere at the sP(5, K) line, while the minimum range R_{min} is attained in tropical atmosphere at the aP(7, 3) line. Our calculations show that for a signal-to-noise ratio exceeding 10, the values of R_{min} and R_{max} are 2.5 and 10 km, respectively.

It should be noted that the backward scattering coefficient β_λ in the ammonia laser range at sea level varies from 1.9×10^{-6} to 2.5×10^{-6} m^{-1} sr^{-1}, [20], while for CO_2 laser it is smaller by a factor of 1.3. According to measurements made in [29] at various lines of the CO_2 laser, the coefficient $\beta_\lambda = 5 \times 10^{-8} - 2.5 \times 10^{-7}$ m^{-1} sr^{-1}, i.e., is ten times higher in the ammonia laser than in the CO_2 laser. However, this

advantage of ammonia laser is partially lost due to a low sensitivity of the KRT detector and low transmission of the atmosphere.

4.2 Lidar sensitivity

The sensitivity of the lidar was determined by carrying out calculations for Freon-11 molecules having an intense absorption band in the range 11.364 – 12.346 μm (Fig. 4a). Arrows in Fig. 4 show the wavelengths of 9 ammonia laser lines falling in this range, while Fig. 4b shows transmission of the standard atmosphere. Table 3 shows the main parameters of these lines. It can be seen that the interfering natural gases have very small absorption cross sections. In other words, the third term need not be taken into account in formula (7). According to the selection rules for optimal wavelengths [30], the sP(7, K) and aP(4, 2) lines with attenuation coefficients 0.24 and 0.44 km^{-1}, respectively, in standard atmosphere can be discarded right away during sensing of Freon-11. In principle, the remaining lines can be used for sensing of Freon-11. The sensitivity S of the lidar at a distance of 1 km (shown in Table 3 for each line) was calculated for a signal-to-noise ratio equal to 200 per pulse. One can see that the minimum concentration measured by a lidar at the sP(6, K) line is equal to 6×10^{-7} % for a spatial resolution of 67 m, which corresponds to a laser pulse duration of 446 ns. The high-intensity lines 3 and 4 (see Table 3) can be used for sensing Freon-11 having low concentrations of the order of 8×10^{-7} % and 6×10^{-7} %, respectively. However, these lines cannot be used for sensing concentrations higher than 7.2×10^{-7} % and 6×10^{-7} % because of a strong attenuation ($\alpha_\lambda = 1.1$ km^{-1}) of the lidar signal due to absorption by Freon-11 itself. Weaker lines 5, 6, 7 and 8 are suitable for sensing higher concentrations of the order of 3×10^{-5} %, 3.5×10^{-5} %, 4.5×10^{-5} % and 6.5×10^{-5} %, respectively. A strong attenuation of the lidar signal due to absorption by the atmosphere itself renders these lines unsuitable for sensing concentrations lower than 3.2×10^{-6} %, 3.6×10^{-6} %, 4.7×10^{-6} % and 7.1×10^{-6} %, respectively.

To determine the sensing error for each line in Table 3, we used relation (6) for a spatial resolution $\Delta R = 150$ m , a relative systematic error $\delta_S = 10$ %, and a number $N_p = 10$ of lidar signal averaging pulses. The results presented in Fig. 5 show that the Freon-11 sensing range for $\delta N = 1$ for high-intensity lines 4 and 3 does not exceed 5.5 km, while the range for weak lines 5, 6, 7 and 8 is more than 8 km. Although line 1 is relatively strong ($E_p \approx 1.4$ J [1]), it may be used for sensing at quite large distances (of the order of 7 km) (Fig. 5).

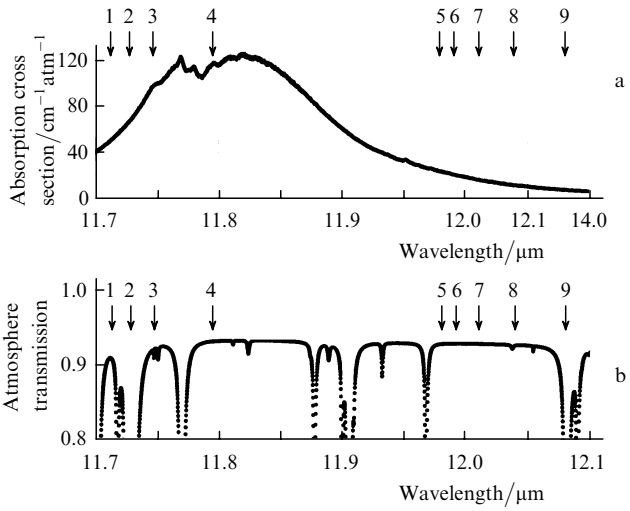

Figure 4. Absorption spectrum of Freon-11 (a) and transmission spectrum of the standard atmosphere along a 1-km long horizontal path at sea level (b). Numbers over arrows indicate the line number in Table 3.

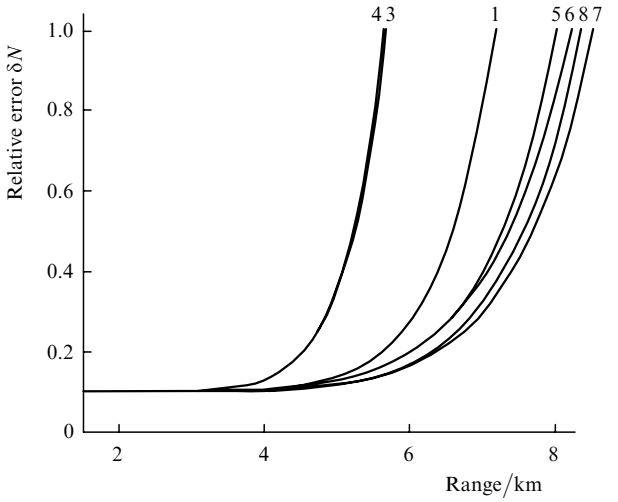

Figure 5. Relative error in measurements of concentration of Freon-11 at various lines of ammonia laser. Numbers over curves indicate the line number in Table 3.

5. Conclusions

Thus, the NH_3-CO_2 lidar is highly sensitive for detecing various materials (Freons, toxins, organic gases and chemical agents). The sensing of these materials can be carried

Table 3.

Line number	Line	λ/μm	E_p/J	α/km^{-1}	Absorption cross section/cm^{-1} atm^{-1}				$S/10^{-7}$ % km^{-1}
					Freon-11	O_3	H_2O	CO_2	
1	aP(4, 0)	11.71209	1.4	0.091	49.21	3.15×10^{-4}	1.16×10^{-4}	3.53×10^{-6}	1
2	aP(4, 2)	11.72713	1.3	0.44	66.22	7.27×10^{-4}	8.24×10^{-4}	3.64×10^{-6}	–
3	aP(4, 3)	11.74637	1.1	0.08	96.91	1.51×10^{-4}	9.7×10^{-5}	9.66×10^{-6}	0.5
4	sP(6, K)	11.79418	1.1	0.07	115.73	1.1×10^{-3}	7.82×10^{-5}	6.82×10^{-6}	0.4
5	aP(5, 1)	11.97859	0.9	0.073	23.12	1.03×10^{-3}	8.22×10^{-5}	4.97×10^{-6}	2
6	aP(5, 2)	11.99025	1.1	0.072	20.16	8.35×10^{-4}	8.03×10^{-5}	5.57×10^{-6}	2.5
7	aP(5, 3)	12.01008	1.2	0.076	15.6	1.2×10^{-3}	8.08×10^{-5}	1.28×10^{-5}	3
8	aP(5, 4)	12.03872	0.9	0.076	10.69	2.04×10^{-3}	8.72×10^{-5}	1.5×10^{-5}	5
9	sP(7, K)	12.07912	1.25	0.24	6.71	4.61×10^{-3}	3.63×10^{-4}	4.6×10^{-5}	–

out at distances from 2.5 to 10 km depending on the lasing line used for this purpose and atmospheric conditions. A large absorption cross section of Freon-11 at ammonia laser lines allows a high sensitivity of up to 4×10^{-8} km^{-1}. It follows from formula (7) that a Freon-11 concentration up to 5×10^{-6} % can be measured at distances from 5 to 8 km with a spatial resolution of 150 m.

References

1. Vasil'ev B.I., Grasyuk A.Z., et al. *Kvantovaya Elektron.*, **7**, 116 (1980) [*Sov. J. Quantum Electron.*, **10**, 64 (1980)].
2. Vasil'ev B.I., Yastrebkov A.B. *Izv. Ross. Acad. Nauk, Ser. Fiz.*, **58**, 202 (1994).
3. Barabanov V.Yu., Bobkov I.V., et al. Preprint TRINITI No. 0043-A (Troitsk, 1998).
4. Anan'ev V.Yu., Vasil'ev B.I., et al. *Kvantovaya Elektron.*, **30**, 535 (2000) [*Quantum Electron.*, **30**, 535 (2000)].
5. Vasil'ev B.I., Cho Ch.W. *Kvantovaya Elektron.*, **30**, 1105 (2000) [*Quantum Electron.*, **30**, 1105 (2000)].
6. Vasil'ev B.I., Zheltykhin A.A., Mannoun O.M. *Kr. Soobsch. Fiz. FIAN*, (7), 22 (2004).
7. Kol'yakov S.F., Malyavkin L.P. *Kvantovaya Elektron.*, **15**, 212 (1988) [*Sov. J. Quantum Electron.*, **18**,135 (1988)].
8. Andreev Yu.M., Geiko P.P., Sherstov I.V. *Proc. SPIE Int. Soc. Opt. Eng.*, **3983**, 386 (1999).
9. Menyuk N., Killinger D.K., De Feo W.E. *Appl. Opt.*, **24**, 2837 (1985).
10. Andreev Yu.M., Geiko P.P., Samokhvalov I.V. *Opt. Atmos. Okean.*, **16**, 783 (2003).
11. Rothman L.S., Barbe A., et al. *J. Quant. Spectr. Rad. Transfer*, **82**, 5 (2003).
12. Ivashchenko M.V., Sherstov I.V. *Kvantovaya Elektron.*, **30**, 747 (2000) [*Quantum Electron.*, **30**, 747 (2000)].
13. Killinger D.F., Menyuk N. *IEEE J. Quantum Electron.*, **17**, 1917 (1981).
14. Carlisle C.B., van der Laan J.E., et al. *Appl. Opt.*, **34**, 6187 (1995).
15. Killinger D.F., Menyuk N. *Opt. Lett.*, **6**, 301 (1981).
16. Murray E.R. *Opt. Eng.*, **16**, 284 (1977).
17. Vasil'ev B.I. D. Sc. Dissertation (FIAN, Moscow, 1997).
18. Murray E.R., van der Laan J.E. *Appl. Opt.*, **17**, 814 (1978).
19. Force A.P., Killinger D.K., De Feo W.E., Menyuk N. *Appl. Opt.*, **24**, 2837 (1985).
20. Maclatchey R.A., Fenn R.W., Selby G.E.A., Garing J.S., in *Optical Properties of the Atmosphere* (Bedford, Massachusetts: Air Force Cambridge Research Laboratories, 1970).
21. Measures R.M. *Laser Remote Sensing. Fundamentals and Applications* (New York: Wiley and Sons, 1984; Moscow: Mir, 1987).
22. Van de Hulst H.C. *Light Scattering by Small Particles* (New York: John Wiley & Sons Inc., 1957).
23. Zuev V.E., Krekov G.M. *Opticheskie modely atmosphery* (Optical Models of the Atmosphere) (Leningrad: Gidrometeoizdat, 1986).
24. Ansmann A., Riebesell M., et al. *Appl. Phys. B*, **55**, 18 (1992).
25. Kriksunov L.Z. *Spravochnik po osnovam infrakrasnoi tekhniki* (Handbook on Fundamentals of Infrared Technology) (Moscow: Sov. Radio, 1978).
26. Firsov K.M., Kataev M.Yu., Mitsel A.A., Pashnik I.V., Zuev V.V. *J. Quant. Spectr. Rad. Transfer*, **61**, 25 (1999).
27. Zuev V.V., Ramonovski O.A. Deposited in VINITI No. 4675-B87 dated 25.06.87.
28. Halldorsson T., Langerholc J. *Appl. Opt.*, **17**, 240 (1978).
29. Ben-David A. *Appl. Opt.*, **38**, 2616 (1999).
30. Mitsel' A.A. *Opt. Atmos. Okean.*, **5**, 978 (1992).